AGU PUBLICATIONS

Space Weather

RESEARCH ARTICLE
10.1002/2016SW001469

Special Section:
NASA's Living With a Star: Geomagnetically Induced Currents

Understanding GIC in the UK and French high-voltage transmission systems during severe magnetic storms

G. S. Kelly[1], A. Viljanen[2], C. D. Beggan[1], and A. W. P. Thomson[1]

[1]British Geological Survey, Edinburgh, UK, [2]Finnish Meteorological Institute, Helsinki, Finland

Key Points:
- Magnetic variation estimates based on the Dst index can provide scale factors to study extreme events
- GIC are estimated in the French and UK high-voltage grids during recent historical storms
- GIC are sensitive to changing network conditions such as varying line resistances or connectivity

Correspondence to:
G. S. Kelly,
gemk@bgs.ac.uk

Citation:
Kelly, G. S., A. Viljanen, C. D. Beggan, and A. W. P. Thomson (2017), Understanding GIC in the UK and French high-voltage transmission systems during severe magnetic storms, *Space Weather*, *15*, 99–114, doi:10.1002/2016SW001469.

Received 13 JUL 2016
Accepted 29 AUG 2016
Accepted article online 6 SEP 2016
Published online 18 JAN 2017

The authorship of this article has changed. See Acknowledgments.

Abstract The measurement and collection of digital magnetic field data in Europe extends back to the 1970s, providing over 30 years of data for the analysis of severe space weather. Although paper records can potentially extend these data sets back by over a century, few digitized records are currently available for use in extreme studies. Therefore, we rely on theoretical arguments and modeling to elucidate the largest likely variations of the magnetic field. We assess the relationship, during the three largest storms in the digital era, between variations in the horizontal magnetic field and the largest measured *Dst* index to estimate likely magnetic variations for more extreme storms in northern and midlatitude Europe. We examine how geomagnetically induced currents (GIC) flow in the UK and French networks during recent severe storms and analyze the sensitivity of these flows to changes in grid parameters. The maximum GIC computed at any one node in the French and UK grids are 44 A and 208 A, respectively. Sensitivity tests show that while gross changes of the whole network structure, such as disconnecting parts of the network, reduces the mean GIC per node, changes in GIC at individual nodes have distinct behaviors implying that local effects are network dependent and require detailed modeling to sufficiently characterize GIC. In addition, the scale factors we have derived allow GIC results from recent storms to be upscaled to estimate the potential risk to the system from more extreme events, such as the Carrington storm in 1859.

1. Introduction

Electric fields are induced in the ground during geomagnetic storms due to the changing magnetic field within the conductive subsurface. For extreme space weather events these induced electric fields can cause large geomagnetically induced currents (GIC) to flow from the ground into high-voltage power systems and out again at points where the networks offer a low-resistance path for near DC currents [e.g., *Viljanen and Pirjola*, 1994; *Pirjola et al.*, 2005].

The economic impacts of an extreme space weather event could potentially be significant if damage were to occur across many points in a high-voltage power network [e.g., *Radasky*, 2011; *Schulte in den Bümen et al.*, 2014]. For example, in the UK, the 13 March 1989 geomagnetic storm caused damage to two transformers [*Erinmez et al.*, 2002a, 2002b] while, more significantly, the same event resulted in the tripping out of the Quebec transmission network for several hours [*Boteler et al.*, 1989]. Hence, the threat of large GIC is of concern to transmission network operators and governments [e.g., *Cannon*, 2013].

Detailed geophysical studies of geomagnetic storms and GIC, such as *McKay* [2003] and *Turnbull* [2011], have modeled the impact on simplified models of the high-voltage transmission system of the UK. *Thomson et al.* [2005] showed that the measured GIC during the October 2003 storm, which reached 40 A in Central Scotland, could be reproduced by geophysical models of the magnetic and electric fields during the storm, combined with a DC model of the transmission network. This suggests such models can be a useful tool in investigating how large and complex transmission networks respond to space weather.

Pulkkinen et al. [2012] developed scenarios of realistic electric field changes for the UK mainland, based on work from *Thomson et al.* [2011]. Large GIC values were generated using a relatively basic model of the UK power network; therefore, *Beggan et al.* [2013] further investigated potential extreme GIC values using a more sophisticated network model and an improved surface conductivity model, based on lithological constraints. Values of up to 460 A were modeled in one transformer substation, or system node, for a 200 year return level event in the UK.

The sensitivity of GIC to variations in the geophysical conductance models was further checked by *Beggan* [2015], who showed that variations in one- and two-dimensional ground conductivity models tended to be

of second-order importance, in terms of GIC production, compared to the first-order significance of auroral electrojet position and strength—though local ground conductivity details could be important for GIC at some nodes in a network. Note, if we fix the ionospheric source, then the ground conductivity is the major contributor to GIC values.

Viljanen et al. [2014] produced the first mainland Europe-wide model of GIC and of ground conductivity. This also provided an independent analysis of GIC in the UK for recent major storms to be compared with, for example, *Thomson et al.* [2005]. *Viljanen et al.* [2014] also demonstrated the (increasing) latitude dependence of GIC across Europe, previously seen in results for the USA and Canada, and assessed the magnitude of GIC that could occur in Scandinavia, particularly in Norway.

Though no systematic studies of GIC solely for the high-voltage French grid have been carried out, *Torta et al.* [2012] provide extensive research into the potential effects within the Spanish network, located south of and connected to the French system. *Torta et al.* [2012] found that GIC of up to 35 A in one node could be reached during a storm of relatively high intensity.

In this paper we provide context for previous extreme GIC event studies, which were based on extreme value statistical analyses of magnetic variation data caused by auroral electrojet activity [e.g., *Thomson et al.*, 2011]. We do this by using a different approach to estimating extreme magnetic variations, involving the equatorial ring current index, *Dst*, as a proxy for the severity of magnetic storms. *Dst* is particularly interesting for a storm proxy as an estimate has been made of *Dst* during the "Carrington Event" (September 1859) at an average of around −800 nT and a peak of over −1700 nT by *Siscoe et al.* [2006] and *Tsurutani et al.* [2003], respectively. From theoretical arguments *Vasyliūnas* [2011] has suggested a maximum possible *Dst* of −2500 nT.

We therefore examine *Dst* in relation to measured magnetic variations at middle- to higher-latitude European observatories, in order to establish scaling relations between the two. These relationships can then be used to scale historical storm data to investigate how the European transmission system might respond to particularly severe space weather (for example, by assuming the time profile of the magnetic field during recent storms). We use electrical transmission system models for the UK and for France, to compare how latitude variations and network topology impact GIC in both isolated (UK) and more connected (France) systems. We do not need to model the whole European grid when considering France but only take into account some nearest-border stations. A sensitivity analysis, in terms of network parameters and configuration, then helps determine the level of accuracy with which one can specify GIC at particular nodes (that is, transformer substations) in each system. This analysis may help provide network operators, regulatory authorities, and governments with additional information on likely system performance during severe space weather.

Section 2 describes the methodology used to relate *Dst* and magnetic variation at middle to high latitudes, as well as the protocol we use for computing GIC in a high-voltage network, through combining a ground conductivity model and time-varying magnetic field model. Section 3 then details the results obtained from the analysis of recent historical storms and the results of a sensitivity analysis of GIC flows to changes in network parameters and topology. In section 4 we discuss these results, relating them to our current understanding of how such systems behave.

2. Methodology

The first part of this section examines two methods relating *Dst* to magnetic field variations at middle to high latitudes. The second part outlines the methodology used in computing GIC in both the French and UK high-voltage networks. We also describe how we can use the scaling values with measured magnetic data from the three largest storms of the digital era: 13–14 March 1989, 29–31 October 2003, and 9–11 June 1991. The third part describes the various sensitivity analyses which explore how GIC in nodes of a network change as we alter the configuration of the network's resistances and topology.

2.1. Upscaling Magnetic Field Variations Via *Dst*

We investigate two methods for scaling historical storms using measured and theoretical values of the *Dst* index and relate these to measured magnetic field variations at middle to high latitudes.

In terms of measured magnetic variations and *Dst*, prior to the early 1980s, only analogue measurements recorded on paper exist, though these do extend back to the 1840s and contain major magnetic storms such

Table 1. Variation of the Absolute Value of the Horizontal Component (Rounded to the Nearest 10 nT) Recorded at UK (LER: Lerwick and HAD: Hartland) and French (CLF: Chambon-la-Forêt) Observatories During Recent Severe Storms and Their Estimated Size Using the Exponential Extrapolation Method

		H (nT)		
	Dst (nT)	CLF	HAD	LER
Measured				
9 Jun 1991	220	200	780	1750
30 Oct 2003	383	750	920	2500
13 Mar 1989	589	670	1510	2800
Exponential fit				
Siscoe et al. [2006]	800	1100	1800	3350
Tsurutani et al. [2003]	1700	2400	3000	4750
Vasyliūnas [2011]	2500	3600	4000	5600

as the Carrington Event and the May 1921 storm. Unfortunately, it has proven difficult to extract an accurate digital record of these severe storms for use in GIC simulations, due to scaling issues and incomplete data, so we need to rely upon modern records to understand the nature of extreme events. In the digital era, the three most severe magnetic storms (in Europe) occurred in March 1989, June 1991, and October 2003. We do note that fewer magnetometer data exist for the March 1989 event than for October 2003, so there is a somewhat larger uncertainty in the actual strength of the magnetic field across the region.

As the *Dst* index is essentially a proxy of the strength of the equatorial ring current, during a geomagnetic storm at higher latitudes the effect from the ring current is much lower than that at the equator, as much of the measured magnetic disturbance likely arises from highly active auroral electrojets. However, there will be some contribution to the measured magnetic field from the ring current.

We thus examine two alternative methods of scaling historical storms using *Dst*. The first method involves fitting an appropriate trend (in this case an exponential curve) to relate *Dst* and the variation of the measured horizontal field variation. We note that *Dst* can be interpreted as a global measure of energy input into the magnetosphere (e.g., through the Burton-McPherron-Russell equation); hence, some fraction of this energy input then drives auroral current systems at the latitudes we are interested in. For this reason it is not unrealistic to assume that there will be some relationship between measured magnetic variations at middle to high latitudes and *Dst*. The second method assumes a simple physical dipolar ring current model which contributes to the measured magnetic field at higher latitudes as some ratio of the total measured field. We intend to use the *Dst* index as a scaling factor for the temporal variation captured in the *H* values. From both of these models, we are able to provide a set of upscaling factors which, when applied to modern magnetic measurements, could account for "Carrington"-sized or larger events.

We first investigate correspondences between observed total magnetic field variations in the horizontal (denoted *H*) plane and the *Dst* index. We examined the three largest *H* component variations in the UK and France during the digital instrument era and compared them with *Dst*. The three storms and associated *Dst* are given in the first three rows of Table 1 (using the absolute value of *Dst* and *H* variation rounded to 10 nT, for convenience). Note that the timing of the largest *H* variations may not necessarily coincide with the time of peak *Dst*, as the *Dst* index is measuring global activity at an hourly cadence, while *H* is a measure of geomagnetic activity local to each observatory.

Figure 1 shows a scatterplot of peak *H* variations from Chambon-la-Forêt (CLF, geomagnetic coordinates for 2015.0: 49.47°N, 85.78°E), in France and Hartland (HAD: 53.47°N, 80.18°E), and Lerwick (LER: 61.67°N, 88.64°E) observatories in the UK against the largest *Dst* during each storm. There is a clear linear to nonlinear trend, though there are some idiosyncrasies, for example, the 2003 value of *H* at CLF is actually larger than that during the 1989 storm.

We therefore choose to fit a second-order exponential curve (that is, $y = x_0 + x_1 \cdot 10 + x_2 \cdot 10^2$) through the data and extrapolate to larger values of the *Dst* (i.e., the 800, 1700, and 2500 nT values identified in section 1), where the fit includes the origin. The extrapolated values for LER of between 3350 and 5600 nT/min are in the range of those from *Thomson et al.* [2011] who estimated such levels as appropriate for a 200 year return maxima. We note that other trend curves may also be useful in relating *Dst* and measured *H*. Hence, our scale factors must be assumed to have some uncertainty associated with them. However, we note that a linear fit would give unrealistically large values for Lerwick. The final three rows of Table 1 show some extreme values of *Dst* and the corresponding estimated values of *H* variation for each *Dst*.

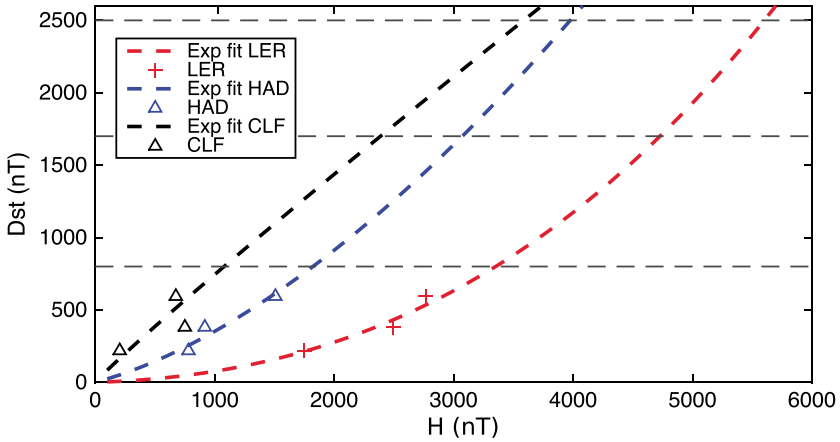

Figure 1. *Dst* versus the Horizontal variation at the Lerwick (LER), Hartland (HAD), and Chambon-la-Forêt (CLF) observatories with an exponential fit to the data. Dashed horizontal lines show 800 nT, 1700 nT, and 2500 nT.

In the second method for estimating *H* variations from measured *Dst*, a simple dipole model of the equatorial ring current is scaled by the *Dst* recorded during the three storms in Table 1. Lerwick has a geomagnetic latitude of around 60°N, so the *Dst* contribution to the observatory *H* variation is relatively small. Table 2 shows the theoretical contribution to the magnetic field from the ring current at Chambon-la-Forêt, Hartland, and Lerwick. Also shown are the (rounded) measured *H* variations recorded for each storm, which are much larger due to the predominant influence of the auroral electrojet at these latitudes.

During the March 1989 storm, a *Dst* of 589 nT, gives a theoretical value of horizontal (north pointing) field strength of 275 nT at Lerwick observatory. The total measured horizontal field variation was 2800 nT, implying that the ring current contribution was about 10% of the total. For the 1991 storm the ring current contribution was 6%, while for the 2003 storm it was 7%. At HAD and CLF, the contribution from the ring current was much larger, up to 72% at CLF, though the average of the three storms is around 50%. Thus, if we take a representative value for the contribution from the ring current to be around 10% at Lerwick, 25% at Hartland, and 50% at Chambon-la-Forêt, we can estimate the ring current contribution to the *H* component variation for other storms for which *Dst* is known or estimated.

Using this simple ring current model factor of 10% for Lerwick, a *Dst* of 800 nT would give a horizontal magnetic field of 375 nT at Lerwick which implies a total horizontal magnetic field variation on the order of 3750 nT. For the 1700 nT and 2500 nT *Dst* scenarios, the magnetic field variations are larger than the values suggested in Table 1 from the exponential fit. For a *Dst* of 2500 nT, the value for the *H* variation of 11,700 nT is over 70% of the main field magnitude at this location, which may be regarded as physically unrealistic.

Table 2. Variation of the Horizontal Component (Rounded to the Nearest 10 nT) Recorded During Three Severe Storms and the Contribution From the Ring Current (RC) at Each Observatory[a]

	Dst (nT)	RC	*H* (nT) CLF	(%) Ratio	RC	*H* (nT) HAD	(%) Ratio	RC	*H* (nT) LER	(%) Ratio
Measured										
9 Jun 1991	220	142	200	71.0	133	780	17.1	105	1750	6.0
30 Oct 2003	383	247	750	32.9	232	920	25.2	175	2500	7.0
13 Mar 1989	589	380	670	56.7	358	1510	23.7	275	2800	9.8
Ring current										
Siscoe et al. [2006]	800	515	1030	50	486	1944	25	375	3750	10
Tsurutani et al. [2003]	1700	1100	2200	50	1033	4132	25	795	7950	10
Vasyliūnas [2011]	2500	1610	3220	50	1520	6080	25	1170	11700	10

[a]Also shown are the extrapolated variations to extreme *Dst* scenarios assuming the ring current model.

Table 3. Scale Factors Relating Modern Measured Data During Known Storms and Hypothesized Extreme Events, Through the *Dst* Index

		Scale Factor		
	Dst (nT)	CLF	HAD	LER
Exponential fit				
Oct 2003	1700	3.2	3.3	1.9
Mar 1989	2500	5.4	2.6	2.0
Ring current				
Oct 2003	1700	2.9	4.5	3.2
Mar 1989	2500	4.8	4.0	4.2

Finally, from the analysis in this section, we can use the maximum estimated values of magnetic field variation in Tables 1 and 2 to give a scaling factor for the historical storms in the digital era. For example, a simple linear scaling of the magnetic field values would suggest (from Table 1) that to adequately scale the March 1989 storm at CLF to a theoretical maximum *Dst* of 2500 nT, the magnetic field values should be multiplied by $3600/670 = 5.4$.

We chose to scale the October 2003 storm to a *Dst* of 1700 nT and the March 1989 storm to 2500 nT. Table 3 shows the scaling factors for both scenarios at all three observatories for both the exponential fit and ring current estimates explained above; we find that the scaling values range between 1.9 and 5.4.

2.2. Calculating GIC in Electrical Transmission Systems

We combine a model of the ground conductivity of the area with the spatial and temporal measurements of the horizontal magnetic field (sampled at 1 min intervals) to compute the surface electric field. A model of the high-voltage power grid and its nodes (or transformers) is then used, which describes the position of the transmission lines and the grounding points. The voltages along each transmission line arising from the surface electrical field are integrated and inverted to calculate GIC in each node. In this study we base our ground conductivity model on the work of *Ádám et al.* [2012] and for brevity show results from historical magnetic field data from the two largest recent storms of 29–30 October 2003 and 13–14 March 1989. We use the method of Spherical Elementary Current Systems (SECS) to interpolate the magnetic field across each region of interest using available magnetic observatory data [*Amm*, 1997].

In order to compute the electric field response in the UK, we use a thin-sheet modeling code based upon the work of *Vasseur and Weidelt* [1977] which has been employed in several previous studies [e.g., *McKay*, 2003; *Thomson et al.*, 2005; *Beggan et al.*, 2013]. The code determines the surface electric field arising at a particular frequency (in this case 1.67×10^{-3} Hz, based on using a period of 600 s) from conductivity models of the surface and subsurface, though we point out that using only one frequency does not yield a full time-domain response. We take the surface model of conductivity from *Ádám et al.* [2012] and use a simplified 1-D model of the conductivity at depth using a single representative block from the *Ádám et al.* [2012] model.

Using a series of Green's functions and integrals, a two-dimensional thin-sheet shallow approximation of the conductance can be used to model the effect that conductivity variations have on redistributing regional or "normal" currents induced elsewhere (for example, in the sea). The surface layer can be regarded as an infinitely thin sheet of finite laterally variable conductance, across which certain boundary conditions apply. A horizontal magnetic field will induce an electric field in the subsurface which creates a discontinuity current sheet at the surface. Hence, the thin-sheet model includes the effect that lateral conductivity variations will have on redistributing regional currents induced elsewhere. A period of 600 s is used, as a previous study [*McKay*, 2003] showed that it best matches the recorded GIC from four sites in Scotland during the 2003 storm.

In terms of ground conductivity for France, we apply the same local 1-D (layered) ground conductivity models as within the EURISGIC (European Risk from Geomagnetically Induced Currents) project [*Viljanen*, 2011]. We note that the calculation of the electric field in France is based on a local 1-D assumption. It follows that close to boundaries of different conductivity blocks the spatial variation of the field cannot be modeled in a fully accurate way. On the other hand, the electric field is always integrated along power lines to determine voltages between nodes. This means that small-scale variations of the field are thus less important. The electric field response in France was computed using the frequency domain method which incorporates all the time variations of the magnetic field.

We used the approach of *Lehtinen and Pirjola* [1985], based on Ohm's and Kirchoff's laws, to calculate the size of GIC entering and exiting the earthed high-voltage network at the *n* earthed nodes:

$$\mathbf{I_e} = (\mathbf{1} + \mathbf{Y_n Z_e})^{-1} \mathbf{J_e} \quad (1)$$

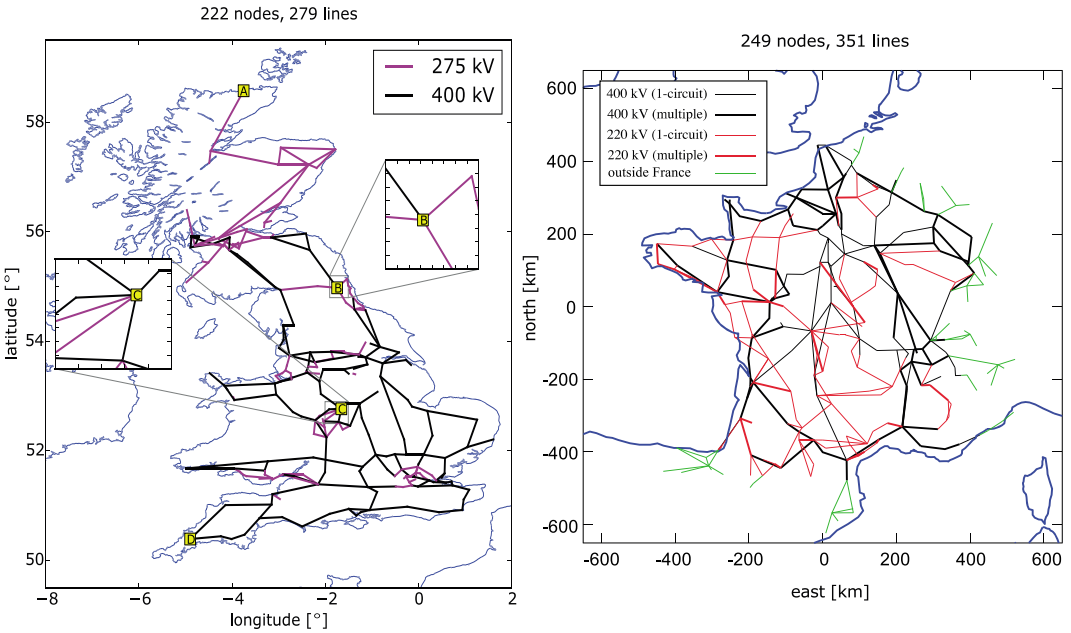

Figure 2. The EURISGIC power transmission networks of the (left) UK and (right) France. Line voltages are color coded according to the legend. The four stations used in the sensitivity analysis of the UK grid are identified by letters A, B, C, and D.

where $\mathbf{J_e}$ is the geovoltage between nodes, $\mathbf{Z_e}$ is the earthing impedance matrix including the earthing resistances of the system. $\mathbf{Y_n}$ is the network admittance matrix and $\mathbf{I_e}$ is the GIC at each node.

For consistency in the comparison of results between the countries, we use the pan-European high-voltage network model developed during the EURISGIC project and described by *Viljanen et al.* [2012]. It includes transmission lines at the voltage level 200 kV and above and is compiled from various sources, including the map of the European interconnected network by ENTSO-E (European Network of Transmission System Operators for Electricity) issued in 2010, and individual maps of nations and existing models from previous local studies. There are several simplifying assumptions in the model, but this network is designed to provide a good representation of a large-scale power grid. The power grid models for the UK and France used in this study are shown in Figure 2; note that all connections in the UK are assumed to be one circuit.

The UK has 222 nodes with 279 connections in total, while in France about 200 nodes and 320 transmission lines have been included. As the French grid has AC connections to neighboring countries we also include the nearest substations to the French border and their nearest neighbors to avoid artificial enhancements of GIC at the French border; these terminating connections are also shown in green in Figure 2. A value of 0.5 Ω is used for the earthing resistance of each node (based on, e.g., *Viljanen et al.* [2012] and *McKay* [2003]), which is the sum of the actual grounding resistance and transformer resistance. We have no information of possible autotransformers, full-wound transformers, or other more complex cases, so we have assumed that all nodes are "simple"; i.e., a three-phase power transmission line is connected to a transformer with a neutral point into the ground.

2.3. Sensitivity of System and Nodal GIC to Network Changes

In order to assess the sensitivity of modeled GIC in a system to changes in network configuration, we investigate three scenarios showing results solely from the UK network. In particular, we investigate (1) varying the earthing resistance of all nodes in the network, (2) varying all line resistances, and (3) removing some lines from the network. We investigate the effect these changes have both on the GIC in the network as a whole, and at four individual sites, as identified in Figure 2 (labeled A to D).

These four sites are chosen to represent different aspects of the network. Site A is an isolated node at the far north of the grid with only one connection, Site B has four connections radiating away to the cardinal points, Site C is a well-connected node (with six connections) near the center of the network, and Site D is a corner

node with only two connections at the far south of the grid. We note that a similar study undertaken for nodes in France gave broadly similar results, when expressed in normalized terms (not shown).

As noted, a lack of available information about the types of transformers at each node (i.e., transformer substation) leads us to assign a constant earthing resistance to each, which is assumed to be 0.5 Ω [see *Viljanen et al.*, 2012]. For our first sensitivity test we evaluate how altering the earthing resistance affects the modeled GIC by multiplying all resistances by a common factor, *C*, taken to be between 0.5 and 5.

The line resistances in the network are calculated by using the known line resistance per unit length at each voltage level (see *Viljanen et al.* [2012] for detail). In the second sensitivity test we therefore vary the per-unit length line resistance across the grid, again by a common factor *C*, while keeping the earthing resistances at their original values. According to the Réseau de Transport d'Électricité (RTE France), the variability of the line resistance per unit length can be of the order 30% across their network, which makes a relevant range for *C* from 0.7 to 1.3.

In the final test we remove lines from the grid in an approximately random way, with every *n*th node disconnected from all others, where *n* is an integer less than the total number of nodes. The only constraint we impose on this scheme is that the four nodes identified in Figure 2 retain their connections to their nearest neighbor so that the effect on GIC at these nodes when distant nodes are disconnected remains relevant.

3. Results

Using the methods described in section 2 we estimate the GIC generated in both the UK and French grids using data from historical storms. We then examine the effect on GIC values when the earthing and line resistances are changed and the topology of the network is altered.

3.1. GIC From Historical Storms

The GIC for each node in the UK and French networks were computed at a cadence of 1 min. As a single number characterizing the network response to space weather, we show the average of absolute GIC per node in each of the UK and French networks throughout the October 2003 and March 1989 storms in Figures 3 (top) and 4 (top), respectively. The time evolution of the average GIC is quite different between the two grids. Though many of the peaks in activity occur at approximately the same time, there are clear differences in fine-scale structure. For example, on 29 October there is a peak in activity around 13:00 UT in France which is largely absent in the UK grid; conversely, there is an extended period of elevated GIC in the UK grid centered around midnight on 30 October which does not appear in the French grid. The difference between the two grids is due to the different time-domain modeling technique. For the UK grid, the thin-sheet method uses only the 600 s period, whereas for the French grid, all periods are included. The peaks in average GIC are larger in the UK network compared to France, which is due to the lower magnitude of the magnetic field variations experienced in France as compared to the UK.

The maximum GIC experienced at any time in the storm by each node is also shown in Figures 3 (bottom row) and 4 (bottom row), though this may not be contemporaneous with the time of the peak in the average of GIC. It is also evident from the spatial distribution that some nodes in either grid are more greatly affected by space weather than others, with nodes at the edges or "corners" of each grid showing largest GIC in general. The maximum GIC at each node are clearly larger in the UK grid than the French grid, which is consistent with the larger average of absolute GIC observed. These differences are likely due to proximity to the auroral oval and the coastal effects that manifest in the thin-sheet modeling of the electric field, compared to the more direct method of *Viljanen and Pirjola* [1994].

These two largest storms can be scaled to match the suggested extreme values of *Dst*, for example, with the October 2003 storm scaled to a *Dst* of 1700 nT, using scaling factors of 3.3 and 4.5, and the March 1989 storm scaled to a value related to a *Dst* of 2500 nT, using a scaling factor of 2.6 and 4.0 (cf. Table 3). Table 4 shows the maximum GIC seen at an individual node and the peak average of absolute GIC for both the unscaled and scaled storm data. We chose to scale using the values at Hartland as it is relatively central both in terms of the scale factors and geographically to the region of interest.

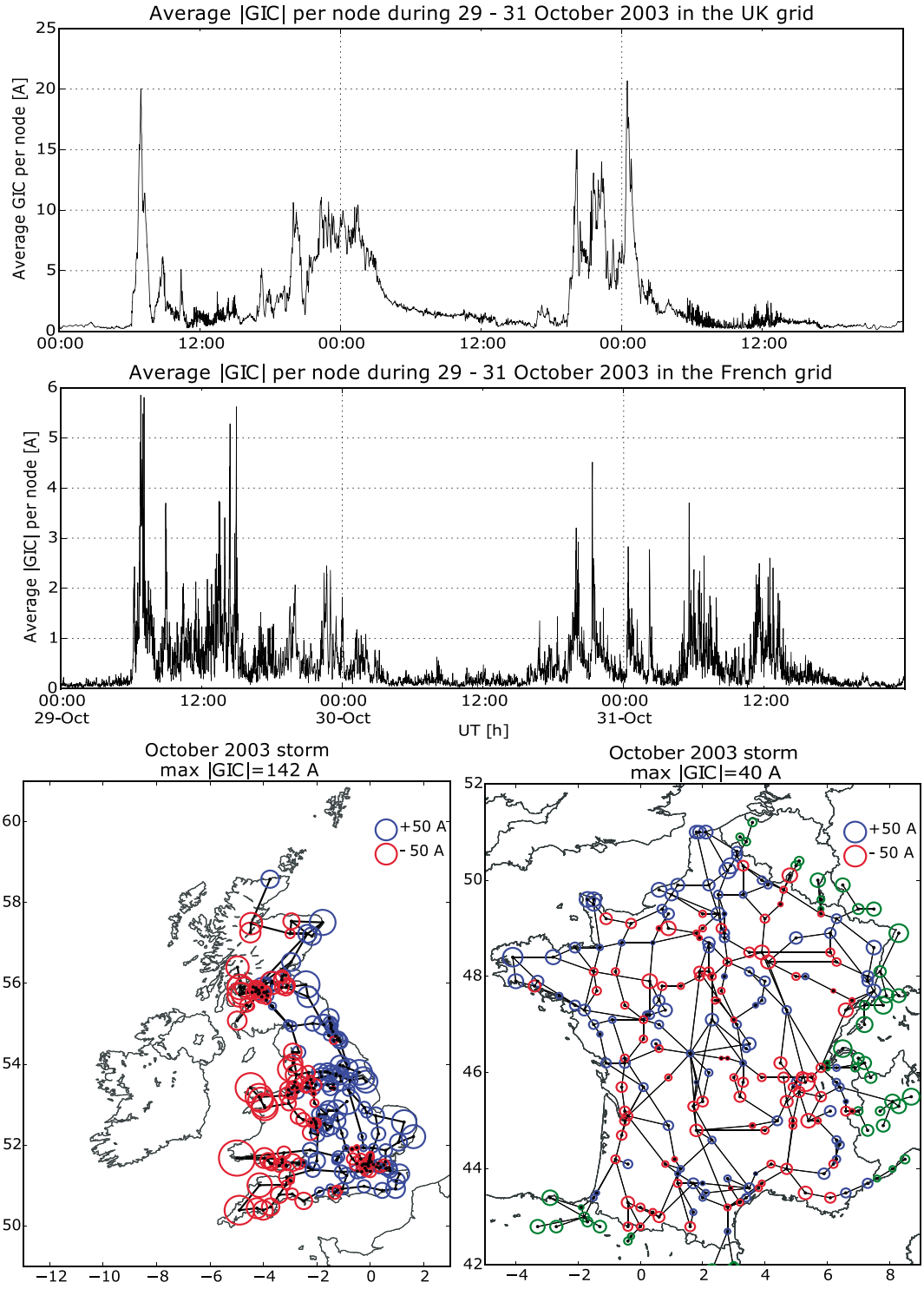

Figure 3. Average |GIC| during the 29–30 October 2003 in the (top) UK and (middle) French networks, and (bottom row) maximum GIC at each node in the (left) UK and (right) French grids at any time during the October 2003 storm. Green circles represent nodes which are outside of the French grid.

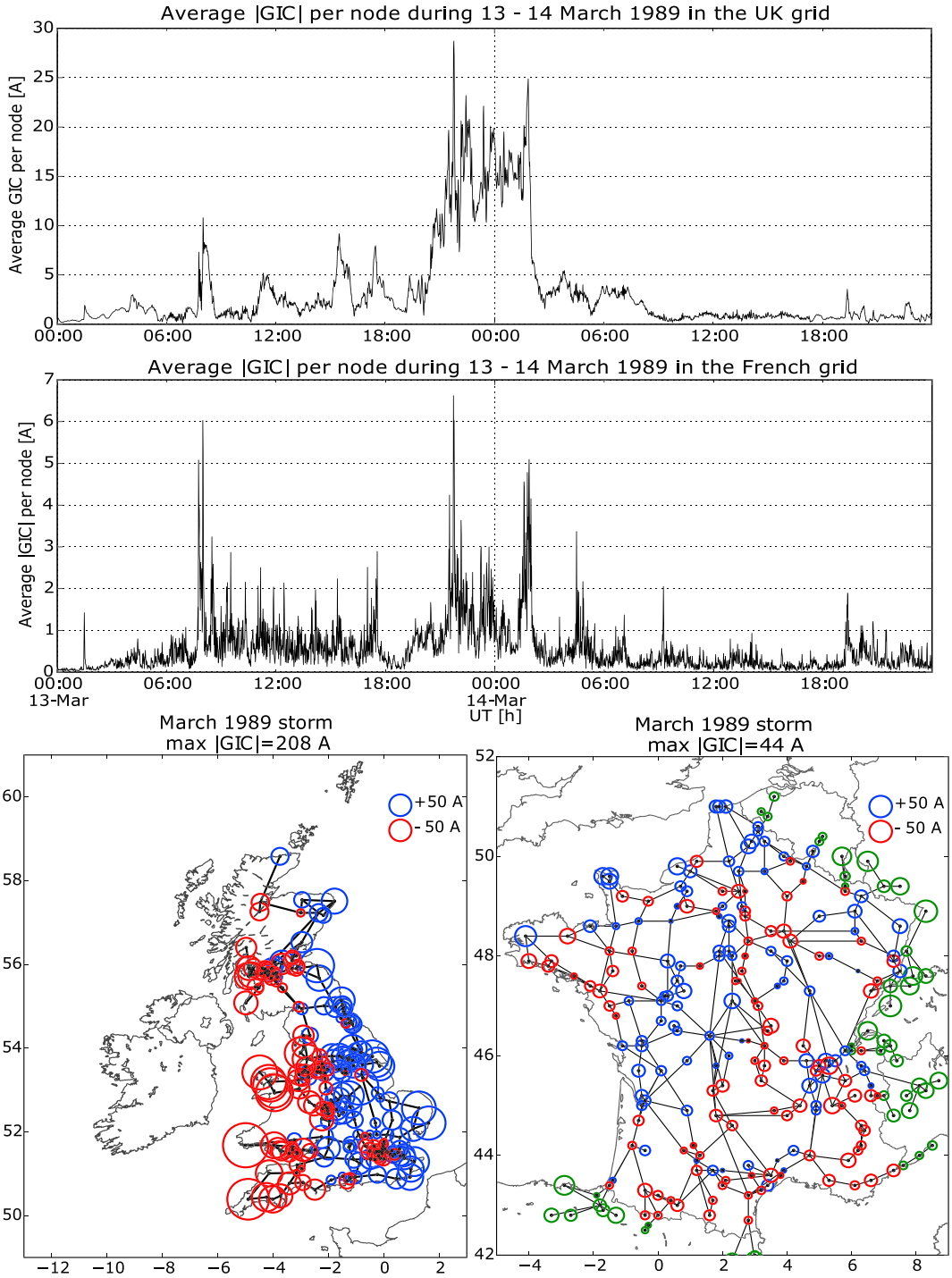

Figure 4. Average |GIC| during the 13–14 March 1989 in the (top) UK and (middle) French networks, and (bottom row) maximum GIC at each node in the (left) UK and (right) French grids at any time during the October 2003 storm. Green circles represent nodes which are outside of the French grid.

Table 4. Estimated GIC in Both UK and French Transmission Grids for Measured and Extrapolated Storm Data[a]

			UK		France	
Storm	*Dst* (nT)	Scaling Factor	Max GIC (A)	Peak Mean (GIC) (A)	Max GIC (A)	Peak Mean (GIC) (A)
Oct 2003	383	-	142	21	40	6
Mar 1989	589	-	208	29	44	7
Exponential fit						
Scaled Oct 2003	1700	3.3	469	68	132	19
Scaled Mar 1989	2500	2.6	541	75	114	17
Ring current						
Scaled Oct 2003	1700	4.5	639	93	180	26
Scaled Mar 1989	2500	4.0	832	115	176	26

[a]Scaled to Hartland using the values from the exponential fit and ring current models.

3.2. Sensitivity Analysis

As described in section 2.3, we also investigated the sensitivity of normalized GIC at each node to changes in the configuration of network parameters. In the following sections we present the results of three tests: varying the earthing resistance (section 3.2.1), varying the line resistance (section 3.2.2), and reducing the number of lines in the network (section 3.2.3). In each case we explored the effect on the whole of the UK grid as well as the effect at the four individual sites highlighted in Figure 2. For brevity we only show the results for the storm in March 1989, but the October 2003 storm gave consistent results. We also performed a similar study for the French grid which again gave similar results in terms of overall behavior (not shown).

3.2.1. Varying the Earthing Resistance Across the Whole Network

The earthing resistance of transformers (in this case the sum of transformer resistances and the actual grounding resistance) varies due to differences in the manner of grounding or the type of transformer in service. We examine here how the GIC at each node in the system changes as the resistance increases (in principle, reducing the total GIC entering the system) or decreases (increasing the GIC entering the system). Figure 5 (top panel) shows normalized sum of absolute GIC, with respect to an unmodified grid, for the network when the earthing resistances are multiplied by a factor, C, between 0.5 and 5. As expected, reducing earthing resistance increases the sum of absolute GIC by a factor of around 38% for a value of $C = 0.5$, while increasing the earthing resistance reduces GIC by a factor of 55% for a value of $C = 5$. However, rather than being a simple offset we see nonlinear variability in the response of GIC in the system with larger changes when $C = 0.5$.

At the four individual sites identified in Figure 2, whose sensitivity data are shown in Figure 5, the effect of changing the earthing resistance is largely consistent with that observed in the whole grid. However, at sites A and B there are occasional peaks in GIC for the altered grids which are, at times, more than thrice as large as the unmodified grid. However, these peaks occur mostly at times when the GIC are small and are actually an effect of the normalization used. Note that in the UK the magnitude of the geoelectric field is used to compute GIC rather than the signed value. This means that the GIC tend to remain either positive or negative at a particular site throughout the modeled storms.

3.2.2. Varying the Line Resistance Across the Whole Network

Line resistance data are available for some networks but for simplicity in the EURISGIC model fixed values of 0.008, 0.022, and 0.0185 Ω km^{-1} were used for 400 kV, 275 kV, and 220 kV lines, respectively [*Viljanen et al.*, 2012, and references therein]. In Figure 6 (top) we show the normalized sum of absolute GIC across all nodes where all the line resistances are multiplied by a common factor, C, between 0.7 and 1.3, and again normalized to the case where $C = 1$. As in the previous section increasing the common resistance factor leads to a decrease in the sum of the GIC, and similarly, a decrease in resistance leads to an overall increase in GIC. There is a similar nonlinear change in the sum of the GIC depending on the reduction of the line resistance.

Figure 6 (bottom) shows that these systematic changes have a mostly consistent impact at the four individual stations. Again sites A and B show occasions when the GIC is approximately doubled, but it is not a consistent offset throughout the whole storm and is most apparent at times when the GIC magnitude is small.

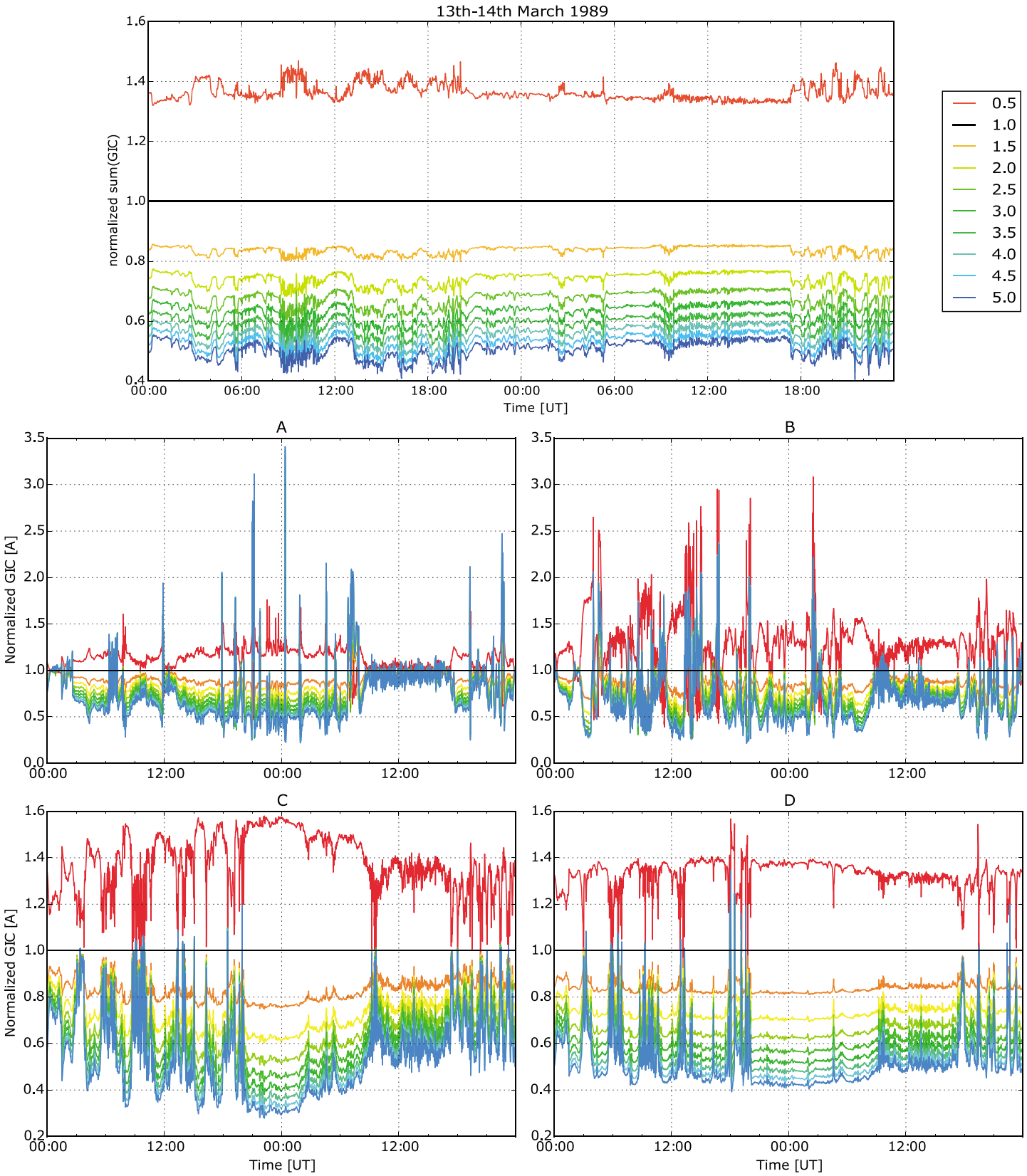

Figure 5. GIC in the UK network, for the 13–14 March 1989 storm, when the earthing resistances in the whole grid are multiplied by a common factor, *C* (indicated by the legend). (top) The sum of absolute GIC in the whole grid, normalized to the sum of absolute GIC when $C = 1$. (bottom) Normalized GIC at the four stations as identified in Figure 2.

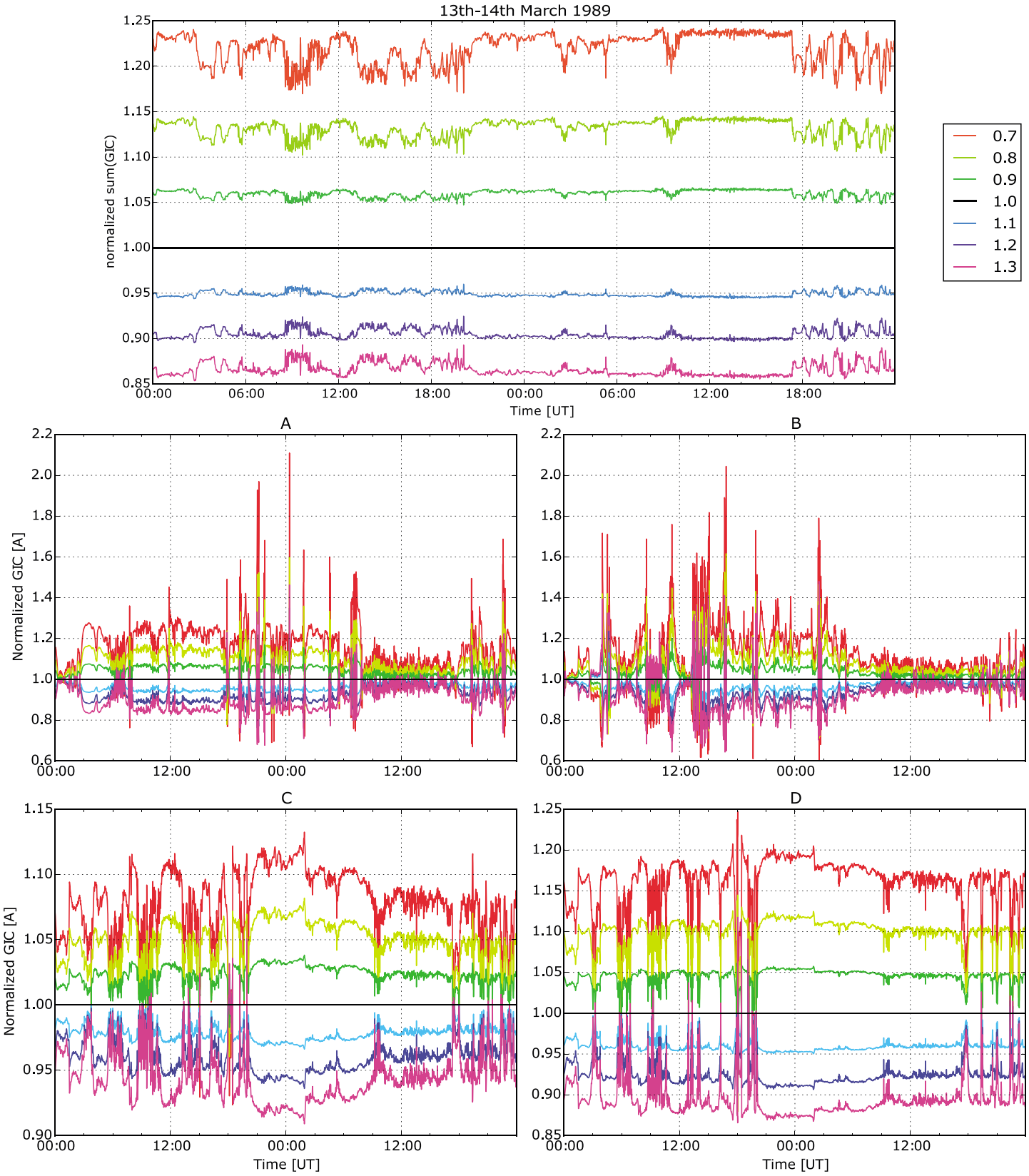

Figure 6. GIC in the UK network, for the 13–14 March 1989 storm, when the line resistances in the whole grid are multiplied by a common factor, *C* (indicated by the legend). (top) The sum of absolute GIC in the whole grid, normalized to the sum of absolute GIC when $C = 1$. (bottom) Normalized GIC at the four stations as identified in Figure 2.

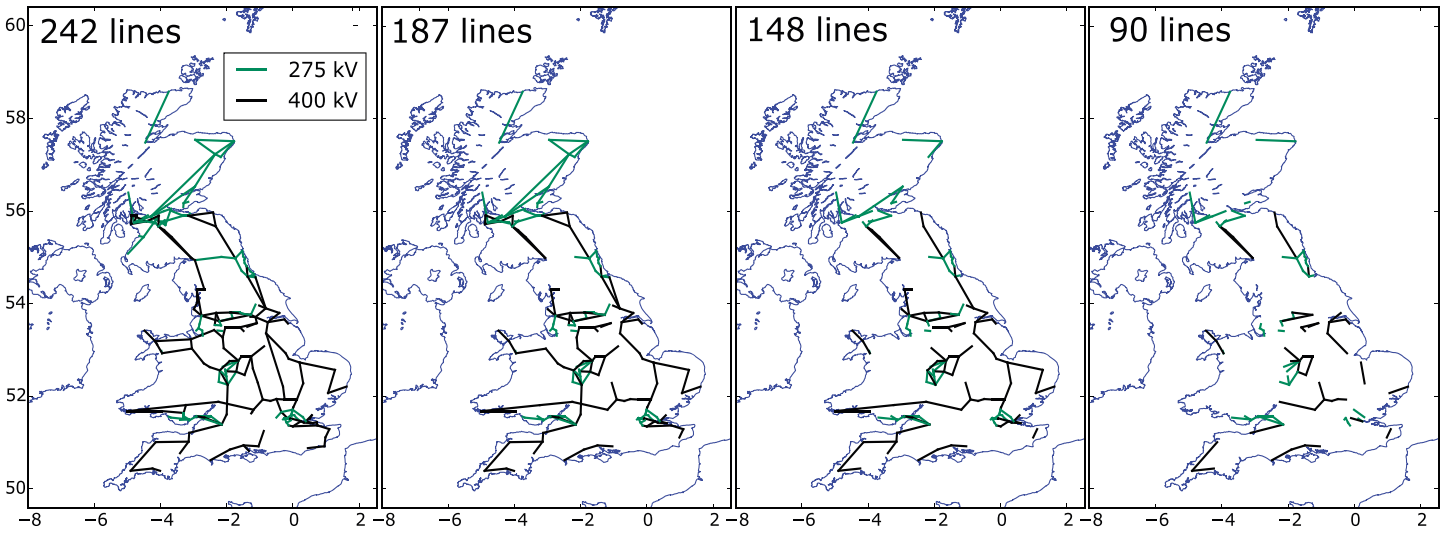

Figure 7. Maps of the UK network as lines are progressively removed in the sensitivity analysis. Numbers in the top left of each plot are the number of lines remaining in the network.

3.2.3. Reducing the Number of Lines in the Network

During an extreme space weather event, one outcome could be that parts of a high-voltage network become disconnected, perhaps due to failure of transformers in the system or automated tripping out of critical infrastructure. The actual behavior of a real-life grid in this scenario would clearly depend on the continued connectivity to power-generating stations as well as on other factors such as frequency control and load-balancing systems. However, we model what happens to the GIC experience at a node as a network structure changes from being nationally connected to regionally isolated. This is achieved by (approximately) randomly removing nodes in the network. Each node was allocated a number between 1 and 222 (ordered by site name), and then every *n*th node is disconnected from the grid, where *n* is an integer less than 222 (the total number of nodes in the UK grid). We then examined the effect across the network as a whole and at the four chosen nodes shown in Figure 2 (right). Figure 7 shows, in this example, that as the number of lines is reduced the grid separates into smaller isolated parts.

The mean of absolute GIC per node in the UK network is shown in Figure 8 (top) for this range of grid configurations. The colors represent the number of lines left in the network starting from the unmodified case (279 lines) down to 90 lines. Only nodes that are still connected are included in the mean at each stage. Overall, as the number of lines is reduced the mean value of GIC in the nodes remaining decreases.

The response to this line removal is noticeably different at the four individual sites shown in Figure 8 (bottom). At Site A there is very little difference in the GIC as we change the number of connected nodes. This is due to its isolated position in the network; node A is only connected to one other node, which in turn only has one other connection; therefore, once this connection has been removed, changes in the rest of the network will not affect node A. It is interesting to note that even in this very simple case, with a single line, we still see relatively large (~30 A) GIC at the peak of the storm. In contrast, at Site B we see a significant reduction in GIC when we reach the two most disconnected cases of 148 and 90 lines in the network. At this point the network on the east coast has become almost completely separated from the rest of the grid, with only very short east-west connections. This causes the GIC to reconfigure and flow differently through the remaining connections.

For node C the changes in GIC appear relatively limited, apart from the final stage when the number of lines in the grid reduces to 90 and the GIC drops. This is a very connected node and the requirement of keeping all of its connections "live" means that there remains a relatively large network surrounding it. This allows GIC to flow through it until it is almost completely isolated. Finally, Site D remains connected into much of the network during the simulation despite its relatively isolated position and the structure of the local network is largely unchanged until most of the lines are removed. Its modeled GIC values do not vary significantly until only the two long lines connecting it are left, when GIC values decrease.

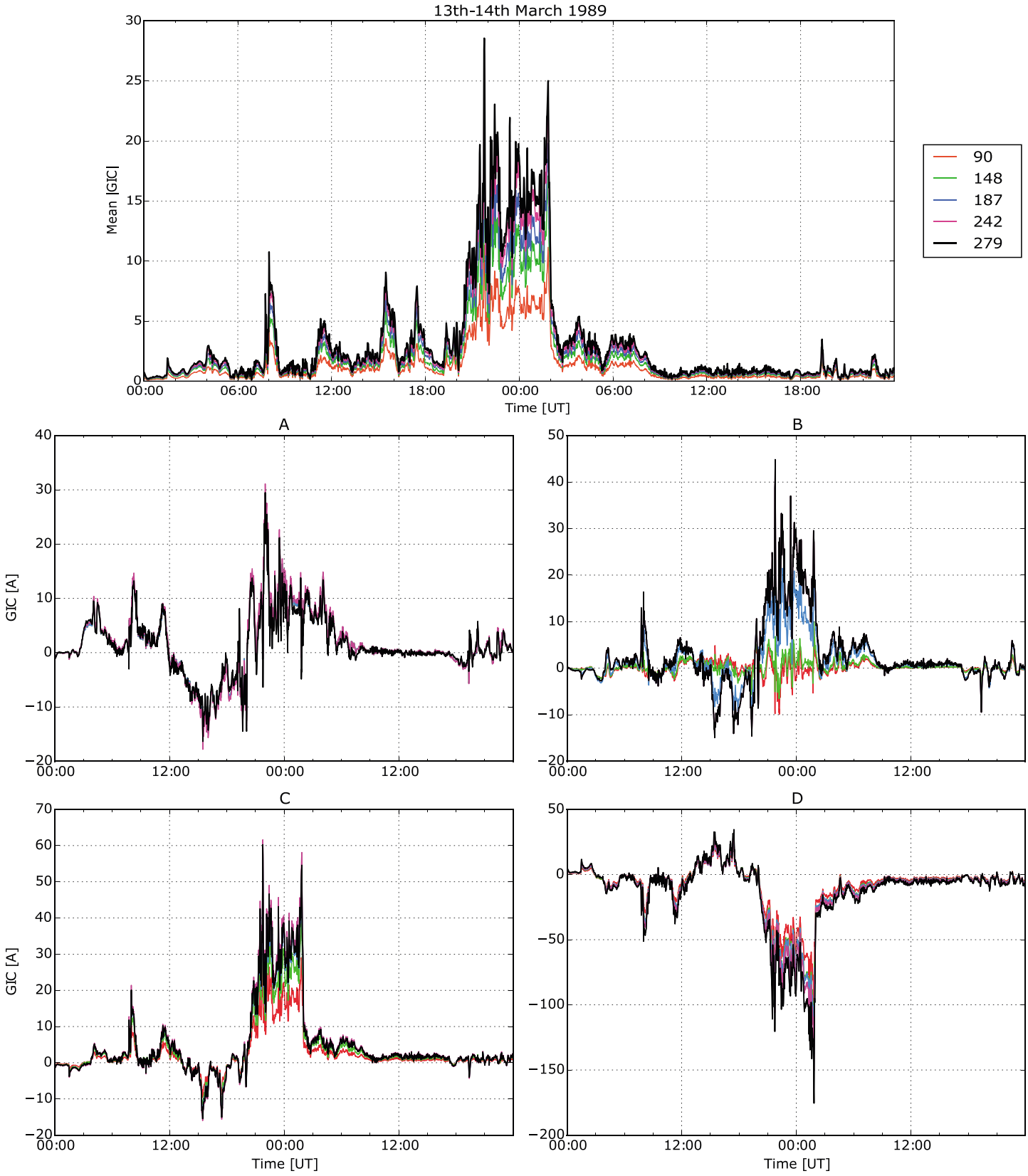

Figure 8. Mean of absolute GIC per node in the (top) UK network and (bottom) GIC at the four stations in Figure 2 as the number of lines in the grid is reduced. The black line shows the mean GIC at each node in the original grid (279 lines), and the key shows the number of lines remaining in the grid at each stage of line removal.

4. Discussion

We have examined two different methods that relate magnetic field variations at middle to high latitudes to the *Dst* index. We have done this as we wish to (a) then make use of research that estimates Carrington level or theoretical maximum *Dst* through the upscaling of GIC simulations for recent magnetic storms with more moderate peak *Dst*, and (b) provide a contrasting analysis to previous extreme event studies that have relied on the inferred strength of the auroral electrojets. The first method uses extrapolation from a second-order exponential fit to data measured at UK and French observatories during recent severe storms. This approach may be open to question in terms of the fitting function used. However, for any fitting function it is reasonable that it should pass through the origin and not extrapolate beyond the maximum strength of the magnetic field. Overall, the maximum *H* values we get from this extrapolation for the largest *Dst* values are in reasonable agreement with previous estimates using extreme value statistics [*Thomson et al.*, 2011].

The second method of upscaling data using *Dst* uses a simple dipole model to estimate the contribution of the ring current to variation in the *H* component observed at any middle- to higher-latitude observatory. The results from this for Lerwick (3750 nT) broadly match the value estimated from the extrapolation method (3350 nT) for $Dst = 800$ nT. For larger *Dst* the estimates diverge, especially for *Dst* of 2500 nT which would lead to 5600 nT using the first method but 11,700 nT using the second. We might also question whether 11,700 nT is perhaps too large to be physically realistic, but we include it as an extreme end-member in any case.

Scaling the March 1989 magnetic field data leads to peak GIC of up to 832 A in the UK and 176 A in France under a $Dst = 2500$ nT scenario. These values do not agree with results shown in previous studies. For example, 832 A is much larger than the 460 A for a 200 year return level in Table 3 of *Beggan et al.* [2013]. This can be explained by the fact that as estimated, the ring current contribution to the magnetic variation is rather small. Hence, the dominating contribution comes from the electrojet, whose amplitude does not directly follow *Dst* meaning the extreme values estimated here are obviously too large. In addition, *Beggan et al.* [2013] used a different network model with 695 nodes and 1178 connections which makes a direct comparison invalid.

The differences in GIC between UK and France are due to a number of factors. Primarily, the conductivity across the two regions is quite different, and the UK is particularly affected by the conductivity contrast at the coast. The regions also experience different variations in the magnetic field magnitude during storms due to their different proximity to the auroral electrojet and ring current. The electrojet is still obviously more important due to the much faster magnetic field variations it induces compared to the ring current. Finally, there are topological differences in each grid in terms of the number of connections, positions, and length of electrical lines.

We also examined the sensitivity of GIC in both grids to variations in electrical parameters such as the earthing and line resistances and the changes in the connectivity of the network. When the earthing and line resistance were increased both changes led to a decrease in GIC as expected. An increase of around 38% in GIC was observed when the earthing resistance was halved while a decrease of about 55% was seen when the resistance was increased fivefold. For similar relative variations in line resistance we find the change in GIC to be somewhat smaller. In this case, individual sites were affected in broadly the same manner as in the overall grid.

When connecting lines are randomly removed, the mean value of GIC in the remaining nodes reduces as the grid becomes more disconnected. However, when we examined how this affected individual sites, it appears that local connections have a dominant effect on the size of GIC at each site. As the network becomes more fractured, the GIC at each site changes in an idiosyncratic manner. For example, at site B GIC reduced once its long E-W connections disappeared, causing the polarity of the GIC to subsequently reverse.

These observations suggest that the behavior of individual nodes in a network are strongly dependent on the relative connectivity to other locations. Hence, it may not be obvious how GIC in a real network might respond to isolation (planned or unplanned) during a severe space weather event.

5. Conclusion

We examined two methods for scaling magnetic field variations at middle to high latitudes using the measured and theoretical maxima of *Dst*. These give peak horizontal magnetic variations that agree reasonably well with the results of other extrapolation techniques in the literature. The scale factors we have calculated

(Tables 3 and 4) can be used to rescale the results given in Figures 3, 4, and 8 to examine what may occur when Carrington-like or larger magnetic storms occur, assuming the time profile of events such as the storms of March 1989 and October 2003.

In addition, we conducted three experiments to examine how GIC vary when changes are made to fundamental properties of the grid such as the earthing and line resistance parameters. System and nodal GIC become smaller as line and earthing resistances increase and larger when these parameters are decreased. Disconnecting parts of the network led to smaller GIC on average, though individual sites all showed different behavior dependent on their setting, location, and connectivity.

Acknowledgments
The authors thank EDF Energy for support. This manuscript reflects the individual views of the authors, and the results and views do not necessarily reflect the views of any funders or the institutions with which the authors are affiliated. Alexis Ruffenach was the last author on the accepted version of the paper, but was removed by agreement of all the original authors. We acknowledge the World Data Centre (WDC) for Geomagnetism, Edinburgh, and all the institutes who operate observatories and submit data to the WDC. The following organizations are thanked for supporting the observatories used in this study: Institut Royal Meteorologique de Belgique, Belgium; Institut de Physique du Globe de Paris, France; the Irish Meteorological Service, Ireland, and British Geological Survey, United Kingdom. This study also benefited from the EURISGIC project that received funding from the European Community's Seventh Framework Programme (FP7/2007-2013) under grant agreement 260330 and from the NERC New Investigators grant NE/J004693/1. This article is published with the permission of the Executive Director of the British Geological Survey (NERC).

References

Ádám, A., E. Prácser, and V. Wesztergom (2012), Estimation of the Electric Resistivity Distribution (EURHOM) in the European lithosphere in the frame of the EURISGIC WP2 project, *Acta Geod. Geophys. Hungarica*, *47*(4), 377–387, doi:10.1556/AGeod.47.2012.4.1.

Amm, O. (1997), Ionospheric elementary current systems in spherical coordinates and their application, *J. Geomag. Geoelectr.*, *49*, 947–955.

Beggan, C. (2015), Sensitivity of geomagnetically induced currents to varying auroral electrojet and conductivity models, *Earth Planets Space*, *67*(1), 1–12, doi:10.1186/s40623-014-0168-9.

Beggan, C. D., D. Beamish, A. Richards, G. S. Kelly, and A. W. P. Thomson (2013), Prediction of extreme geomagnetically induced currents in the UK high-voltage network, *Space Weather*, *11*, 407–419, doi:10.1002/swe.20065.

Boteler, D. H., R. M. Shier, T. Watanabe, and R. E. Horita (1989), Effects of geomagnetically induced currents in the BC Hydro 500 kV system, *IEEE Trans. Power Delivery*, *4*(1), 818–823.

Cannon, P. (2013), Extreme space weather: Impacts on engineered systems and infrastructure, Tech. Rep., Royal Academy of Engineering, London.

Erinmez, I. A., J. G. Kappenman, and W. A. Radasky (2002a), Management of the geomagnetically induced current risks on the national grid company's electric power transmission system, *J. Atmos. Sol. Terr. Phys.*, *64*, 743–756.

Erinmez, I. A., S. Majithia, C. Rogers, T. Yasuhiro, S. Ogawa, H. Swahn, and J. G. Kappenman (2002b), Application of modelling techniques to assess geomagnetically induced current risks on the NGC transmission system, in *International Council on Large Electrical Systems CIGRE*, vol. SC 39, pp. 1–10, CIGRE, Paris.

Lehtinen, M., and R. Pirjola (1985), Currents produced in earthed conductor networks by geomagnetically-induced electric fields, *Ann. Geophys.*, *4*, 479–484.

McKay, A. (2003), Geoelectric fields and geomagnetically induced currents in the United Kingdom, PhD thesis, Edinburgh, U. K.

Pirjola, R., K. Kauristie, H. Lappalainen, A. Viljanen, and A. Pulkkinen (2005), Space weather risk, *Space Weather*, *3*, S02A02, doi:10.1029/2004SW000112.

Pulkkinen, A., E. Bernabeu, J. Eichner, C. Beggan, and A. Thomson (2012), Generation of 100-year geomagnetically induced current scenarios, *Space Weather*, *10*, S04003, doi:10.1029/2011SW000750.

Radasky, W. A. (2011), Overview of the impact of intense geomagnetic storms on the U.S. high voltage power grid, in *IEEE International Symposium on Electromagnetic Compatibility*, pp. 300–305, IEEE Conference Publications., California, doi:10.1109/ISEMC.2011.6038326.

Schulte in den Bümen, H., D. Moran, M. Lenzen, I. Cairns, and A. Steenge (2014), How severe space weather can disrupt global supply chains, *Nat. Hazards Earth Syst. Sci.*, *14*, 4463–4486, doi:10.5194/nhessd-2-4463-2014.

Siscoe, G., N. U. Crooker, and C. Clauer (2006), Dst of the Carrington storm of 1859, *Adv. Space Res.*, *38*(2), 173–179, doi:10.1016/j.asr.2005.02.102.

Thomson, A. W. P., A. J. McKay, E. Clarke, and S. J. Reay (2005), Surface electric fields and geomagnetically induced currents in the Scottish Power grid during the 30 October 2003 geomagnetic storm, *Space Weather*, *3*, S11002, doi:10.1029/2005SW000156.

Thomson, A. W. P., E. Dawson, and S. Reay (2011), Geomagnetic extreme statistics for Europe, *Space Weather*, *9*, S10001, doi:10.1029/2011SW000696.

Torta, J. M., L. Serrano, J. R. Regue, A. M. Sanchez, and E. Roldan (2012), Geomagnetically induced currents in a power grid of northeastern Spain, *Space Weather*, *10*, S06002, doi:10.1029/2012SW000793.

Tsurutani, B., W. Gonzalez, G. Lakhina, and S. Alex (2003), The extreme magnetic storm of 1–2 September 1859, *J. Geophys. Res.*, *108*(A7), 1268, doi:10.1029/2002JA009504.

Turnbull, K. (2011), Modelling of geomagnetically induced currents in the United Kingdom, PhD thesis, Lancaster, U. K.

Vasseur, G., and P. Weidelt (1977), Bimodal electromagnetic induction in non-uniform thin sheets with an application to the northern Pyrenean induction anomaly, *Geophys. J. R. Astron. Soc.*, *51*, 669–690.

Vasyliūnas, V. M. (2011), The largest imaginable magnetic storm, *J. Atmos. Sol Terr. Phys.*, *73*(11), 1444–1446, doi:10.1016/j.jastp.2010.05.012.

Viljanen, A. (2011), European project to improve models of geomagnetically induced currents, *Space Weather*, *9*, S07007, doi:10.1029/2011SW000680.

Viljanen, A., and R. Pirjola (1994), Geomagnetically induced currents in the Finnish high-voltage power system, *Surv. Geophys.*, *15*(4), 383–408, doi:10.1007/BF00665999.

Viljanen, A., R. Pirjola, M. Wik, A. Ádám, E. Prácser, Y. Sakharov, and J. Katkalov (2012), Continental scale modelling of geomagnetically induced currents, *J. Space Weather Space Clim.*, *2*, A17, doi:10.1051/swsc/2012017.

Viljanen, A., R. Pirjola, E. Prácser, J. Katkalov, and M. Wik (2014), Geomagnetically induced currents in Europe, *J. Space Weather Space Clim.*, *4*, A09, doi:10.1051/swsc/2014006.